Calculation of Surface Acoustic Waves on a Piezoelectric Substrate using Amazon™ Cloud Computing

U. Vogel[*1,2], M. Spindler[1], A.Winkler[1], T. Gemming[1]
[1]IFW Dresden, SAWLab Saxony, PO Box 270116, D-01171 Dresden, Germany
[2]TU Dresden, Institute of Materials Science, D-01069 Dresden, Germany

*Corresponding author: u.vogel@ifw-dresden.de

Abstract:

The excitation of surface acoustic waves (SAWs) on piezoelectric substrates requires profound knowledge of their physical fundamentals as well as dedicated technologies for the device production. As the acoustic wavefield is the basis for various emerging applications including such for microfluidic actuation, it has to be tailored for each task individually. However, the production and measurement of various different SAW-devices is time- and cost-intensive.

In this work, we seek to simulate SAWs for a better understanding and to benchmark the currently available cloud computing possibilities of COMSOL Multiphysics®. By using the additional MEMS module we demonstrate 3D models with reduced geometry to achieve principle information about the wavefield. For a benchmark, a high-speed workstation with limited random-access memory (RAM) is compared to the most potent Amazon™ Cloud Computing (AWS) single-instance machine currently available for COMSOL Multiphysics®.

Keywords: surface acoustic wave, piezoelectric, cloud computing, 3D, $LiNbO_3$, COMSOL Multiphysics®, Amazon Web Services™

1. Introduction

Conventional applications of surface acoustic wave (SAW) devices, including high-frequency filters or radio-frequency identification (RFID) tags, are based on the electrical transmission or resonance behaviour of the used interdigital transducer (IDT) arrangement. In the last 40 years, the research and development of SAW devices for telecommunication [1] was, thus, focussed on the optimization of the electrical behaviour of the IDTs [2]. The properties and shape of the acoustic wavefield, i.e. the lateral distribution of amplitude and phase of the SAW, thereby plays only a minor role. However, the function of emerging applications for SAW devices including microfluidic actuators [3-5] and devices incorporating phononic crystals [6-8] is rather based on the excited wavefield than on the electrical behaviour of the IDTs.

The propagation of SAW excited on piezoelectric substrates as well as their interaction with objects in their path are determined by the solution of the wave equation in the solid, taking into account the anisotropic character of the substrate and the geometric boundary conditions, including the IDT structure, the IDT arrangement and the existence of functional layers. Moreover, the SAW interaction with fluids is determined by the interplay between the wave equation in the solid/fluid half spaces and the Navier-Stokes equation for the fluid half space. Both equations are highly nonlinear and analytic solutions are often not available.

In principle, the finite element method (FEM) represents a suitable alternative for the simulation of SAW propagation and their interaction with fluids, particles or phononic crystals. Various examples for the (quasi) two-dimensional case [9-11] of SAW excitation and propagation or for periodic structures [12,13] were already published. However, the three-dimensional simulation of SAW excitation, propagation and interaction with objects in the acoustic path is still in an initial state with only few results in the literature [14-16]. In addition, the commonly used simplified assumption of plane wave excitation and the associated reduction of the model to two dimensions is not correct when significant diffraction occurs, e.g. for wavelength-to-aperture ratios larger than 0.1, at a high number of finger pairs or for focussed IDT structures. Complex three-dimensional models have to take into account large time- (femtoseconds to milliseconds) and length-scales (nanometers to millimetres), various material properties, a high number of volume elements and optimized solver settings [17]. For this

purpose, even good high-speed workstations are insufficient at this point of time.

COMSOL Multiphysics® 5.1 (Comsol) now renders the use of cloud-based FEM simulation possible. Thereby, the interplay between Comsol and the Amazon Web Services™ (AWS) enables the on-demand availability of high-speed workstations with properties adjustable to the model in use. Moreover, the perspective of even faster available virtual machines could make the simulation of complex 3D SAW excitation, propagation and their interaction with fluids or particles possible in the near future.

In this work, we compare a high-speed personal computer to the fastest available memory optimized Amazon cloud machine (EC2 R3 instance) regarding the simulation of SAW excitation on a piezoelectric substrate.

2. Model description

2.1 Governing equations

SAWs can be modeled using the equations for the piezoelectric effect (1,2), the wave propagation (4) and the charge conservation (3) at the surface of a solid state material [18].

$$\boldsymbol{T_{ij}} = \sum_{kl} \boldsymbol{C^E_{ijkl}} \cdot \boldsymbol{S_{kl}} - \boldsymbol{e^T_{ijk}} \cdot \boldsymbol{E_k} \quad (1)$$

$$\boldsymbol{D_i} = \sum_{jkl} \quad \boldsymbol{e_{ikl}} \cdot \boldsymbol{S_{kl}} + \boldsymbol{\varepsilon^S_{ij}} \cdot \boldsymbol{E_j} \quad (2)$$

$$\sum_{jkl} \boldsymbol{C^E_{ijkl}} \frac{\partial^2 u_l}{\partial x_j \partial x_k} + \sum_{ijk} \boldsymbol{e_{kij}} \frac{\partial^2 V}{\partial x_j \partial x_k} = \boldsymbol{\rho} \frac{\partial^2 u_i}{\partial t^2} \quad (3)$$

$$\sum_{ijk} \boldsymbol{e_{jkl}} \frac{\partial^2 u_l}{\partial x_j \partial x_k} - \sum_{ijk} \boldsymbol{\varepsilon^s_{jk}} \frac{\partial^2 V}{\partial x_j \partial x_k} = \boldsymbol{0} \quad (4)$$

Thereby, T_{ij} is the stress tensor, C_{ijkl} the elasticity tensor, ε_{ijk} represents the piezoelectric matrix, ε_{ij} is the permittivity tensor, E_k the electric field vector, S_{kl} the strain tensor, ρ the mass density, u_i the displacement, V the electrical potential, t the time, x_i the coordinate, and D_i the electrical displacement.

We have simulated a 128°YX-$LiNbO_3$ substrate (128° rotated Y-cut Lithium Niobate with X-propagation direction). The IDT consists of one finger electrode pair located in the middle of the substrate surface. The desired Rayleigh SAW wavelength is set to λ = 150 µm, thus the electrode width is given by $\lambda/4$ = 37.5 µm with an aperture width of 1 mm.

The vertical boundary surfaces are assigned to low-reflecting conditions for P and S waves in order to avoid interferences between non-scattered and scattered waves. In the substrate domain, a weak mechanical Rayleigh damping has been applied with a stiffness parameter of $\beta \approx 10^{-12}$ s. The electrical boundary conditions take into account charge conservation in the whole domain and electrode potential. Thereby, one electrode is addressed with ground potential (V = 0 V) and the other one with a harmonic time dependent potential $V = V_0 sin(2\pi f t)$ with a frequency of f = 26.6 MHz and a voltage amplitude of V_0 = 1 V.

2.2 Material settings

The anisotropic material data for the $LiNbO_3$ substrate were taken from the Comsol material library. The elastic, piezo-mechanical and permittivity constants as well as the mass density are required for this simulation. The 128° YX crystal cut was considered by the application of a rotated coordinate system using Euler angles of (0°, 38°, 0°). Electrode materials as well as the electrode thickness were not included in the simulation and the electrodes were modeled as equipotential planes on the substrate surface**.**

2.5 Mesh settings

As it is necessary to obtain a qualitatively high resolution along the surface, we used an equidistant mapped mesh with an element size of 18.75 µm x 18.51 µm**,** corresponding to 8 mesh elements per wavelength. The surface mapped mesh has been swept through the substrate thickness using 10 elements with an element ratio of 20, see Figure 1.

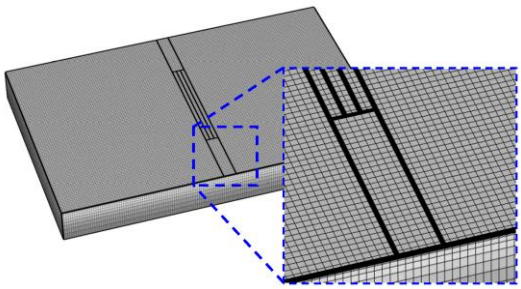

Fig. 1: Mapped mesh consisting of equidistant elements (160 x 108) on the substrate surface (3 x 2 mm²), swept by 10 elements with a ratio of 20 throughout the substrate thickness (300 µm).

Altogether, the high-resolution model consisted of 172.800 hexahedral mesh elements, 39.920 quadrilateral elements, 1.448 edge elements and 20 vertex elements with a total of 5.851.188 degrees of freedom.

2.6 Study settings

A time dependent solver has been chosen with discrete time steps of $\Delta t \approx 6$ ns (1/25 of the oscillation period) for a time range of 186 ns (5 SAW cycles). Additionally, an iterative multigrid solver was attached to achieve better memory efficiency [17].

2.7 Computational settings

The focus of this study is to evaluate the possibilities of Amazon web services, in respect to computing power and time efficiency, and the comparison to a high-speed desktop workstation (Table 1). The addressed virtual machine for cloud computing was the fastest available memory optimized Amazon cloud machine (EC2 R3 instance of the type r3.8xlarge).

Table 1: Comparison Workstation vs. AWS

	Desktop workstation	**AWS r3.8xlarge**
RAM	32 GB	244 GiB
CPU	1x *Intel® Core™ i7-2600 @ 3.4 GHz*	32x *Intel® Xeon™ E5-2670 v2 @ 2.5 GHz*
Disc	1x 2 TB (HDD)	2x 320 GB (SSD)
System	Win 7 x64 SP1	Win Server 2012 6.2

3. Results and discussion

Figure 2 shows the resulting Rayleigh SAW at the end of the simulation, i.e. after a time of 186 ns (5 periods). The color index refers to the vertical mesh displacement (u_3-component of the SAW). The maximum vertical amplitude measured equals 0.128 nm at an input voltage of 1 V.

Beside the main SAW propagation direction (perpendicular to the electrodes), the SAW is also propagating in an angular spectra around the IDTs. However, the amplitude of these wave components is much smaller, which is expected to result from a much lower coupling coefficient for propagation directions differing from the x-direction.

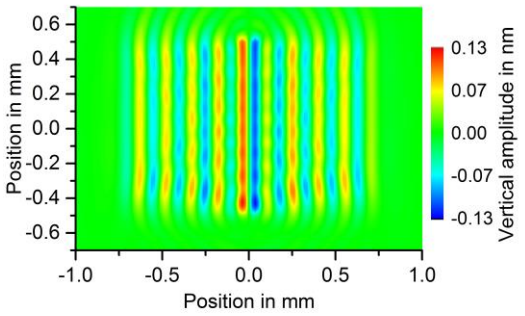

Fig. 2: Rayleigh SAW (vertical surface displacement) generated by harmonic electrical excitation of finger electrode in the middle of the substrate.

Another diffraction effect is visible in Figure 2, namely the diffraction caused by the limited aperture width. For the IDT simulated here, the wavelength-to-aperture ratio measures 0.15, so the assumption of infinite long finger electrodes is not valid and strong diffraction is expected. This is visible by the amplitude variation perpendicular to the IDT propagation direction and a focusing effect of the SAW.

Additionally, the wavefield was found to be not symmetric in the direction perpendicular to the SAW propagation direction. This could be caused by inaccurate material parameters for this crystal cut.

Strong differences between the workstations with respect to their computing power and time efficiency were detected. For the computation of the same model, the workstation needed 6 days and 1 hour for the, whereas the AWS simulated only 2 hours and 30 minutes. As the model required

approximately 60 GB of working memory, it exceeded the available memory of the desktop workstation. Thereby, Comsol used a swap file for intermediate model storage. The data exchange between the swap file and the working memory seems to be the bottleneck of Comsol Multiphysics®, limiting the model size computable in a given time.

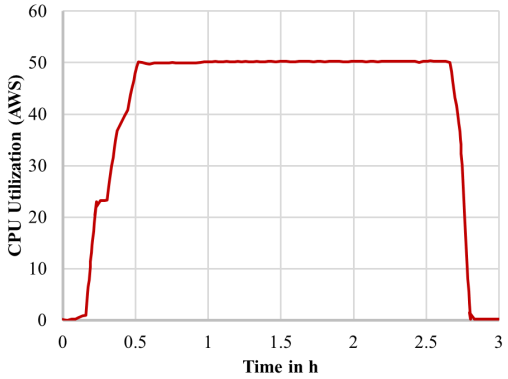

Fig. 3: CPU utilization rate for the AWS workstation.

In Figure 3, the CPU utilization rate for the AWS workstation is displayed, showing a good workload and calculation efficiency. In comparison, the desktop workstation with much less CPUs had an overall CPU utilization rate of below 10%, caused by the insufficient working memory availability.

4. Conclusion

The task-specific tailoring of SAW devices, e.g. for microfluidic actuation, would strongly benefit from the possibility of a-priori 3D simulations. The cloud-based simulation environment of AWS in combination with Comsol Multiphysics® brings the simulation of complex, high-resolution 3D SAW propagation into reach.

Here, we were able to simulate the SAW propagation with a complex – still simplified – model with almost 6 million degrees of freedom, containing an IDT with one finger pair on an anisotropic $LiNbO_3$ substrate in less than 3 hours.

However, we experienced certain difficulties regarding the communication protocols between Comsol multiphysics® and the AWS machine leading to simulation failure and limitations in the model size. Work has to be done here to ensure a stable simulation environment in the future. Additionally, as the available virtual machines can still easily be brought to their limits with anisotropic models such as the one presented here, even faster workstations with larger memory are necessary.

5. References

1. K.-Y. Hashimoto, *Surface acoustic wave devices in telecommunications: Modelling and simulation*, 330, Springer, Berlin/Heidelberg, (2000)

2. M. Spindler, S. B. Menzel, J. Eckert and C. Eggs, Influence of Al on resistance and power durability of Cu-based SAW metallizations, *IOP Conference Series: Materials Science and Engineering*, **8**, 012013 (2010)

3. H. Bruus, J. Dual, J. Hawkes, M. Hill, T. Laurell, J. Nilsson, S. Radel, S. Sadhal and M. Wiklund, Acoustofluidics: Forthcoming Lab on a Chip tutorial series on acoustofluidics: Acoustofluidics-exploiting ultrasonic standing wave forces and acoustic streaming in microfluidic systems for cell and particle manipulation, *Lab on A Chip*, **11**, 3579-3580 (2011)

4. L. Y. Yeo and J. R. Friend, Surface Acoustic Wave Microfluidics, *Annual Review of Fluid Mechanics*, **46**, 379-406 (2014)

5. A. Winkler, S. B. Menzel, H. Schmidt, I. Mönch, A. Jahn and U. Künzelmann, Novel technology for SAW based microfluidic devices with buried interdigital transducer electrodes, *IOP Conference Series: Materials Science and Engineering*, **8**, 012012 (2010)

6. S. Yankin, A. Talbi, Y. Du, J. C. Gerbedoen, V. Preobrazhensky, P. Pernod and O. B. Matar, Finite element analysis and experimental study of surface acoustic wave propagation through two-dimensional pillar-based surface phononic crystal, *Journal of Applied Physics*, **115** (2014)

7. Y. Bourquin, R. Wilson, Y. Zhang, J. Reboud and J. M. Cooper, Phononic Crystals for Shaping Fluids, *Adv. Mater.*, **23**, 1458-1462 (2011)

8. M. Addouche, M. A. Al-Lethawe, A. Choujaa and A. Khelif, Superlensing effect for surface acoustic waves in a pillar-based phononic crystal

with negative refractive index, *Applied Physics Letters*, **105** (2014)
9. S. Zhgoon, D. Tsimbal, A. Shvetsov and K. Bhattacharjee, 3D finite element modeling of real size SAW devices and experimental validation, *Proceedings of the International Ultrasonics Symposium*, Beijing, 1932-1935 (2008)
10. M. M. El Gowini and W. A. Moussa, A Reduced Three Dimensional Model for SAW Sensors Using Finite Element Analysis, *Sensors*, **9**, 9945-9964 (2009)
11. N. Ramakrishnan, A. K. Namdeo, H. B. Nemade and R. P. Palathinkal, Simplified Model for FEM Simulation of SAW Delay Line Sensor, *Procedia Engineering*, **41**, 1022-1027 (2012)
12. A. Stefanescu, A. Muller, A. Dinescu, G. Konstantinidis, A. Cismaru, A. Stavrinidis and D. Neculoiu, FEM analysis of GaN based surface acoustic wave resonators, *Proceedings of the International Semiconductor Conference (CAS)*, Bucharest 177-180 (2011)
13. D. Karim, S. Ballandras, T. Laroche, K. Wagner, J. M. Brice and X. Perois, Finite Element Analysis in Combination with Perfectly Matched Layer to the Numerical Modeling of Acoustic Devices in Piezoelectric Materials, *Applied Mathematics*, **4**, 64-71 (2013)
14. G. Gálik, V. Kutiš and J. Murín, 3D FEM model of piezoelectric SAW sensor, *Proc. 20th Inter. Conf. on Applied Phys. of Cond. Matter (APCOM 2014)*, Bratislava, 316-319 (2014)
15. S. Krishnamurthy, M. Z. Atashbar and K. Kalantar-Zadeh, 3D Modeling and Simulation of SH-SAW Devices Using the Finite Element Method, *Proceedings of the IEEE Sensors Conference*, Atlanta, 357-359 (2007)
16. K. R. S. Sankaranarayanan, V. R. Bhethanabotla and B. Joseph, Finite Element Modeling of Surface Acoustic Wave (Saw) Sensor Responses, *Proceedings of the 3rd International Symposium on Runaway Reactions, Pressure Relief Design, and Effluent Handling*, Ohio, 593f (2005)
17. V. Marra and S. Datta, Two-port Piezoelectric SAW Device (ID: 19155), *Comsol Multiphysics GmbH Application Gallery*, www.comsol.de/model/two-port-piezoelectric-saw-device-19155, (Accessed 01.09.2015)
18. G. S. Chung and D. T. Phan, Finite Element Modeling of Surface Acoustic Waves in Piezoelectric Thin Films, *J Korean Phys Soc*, **57**, 446-450 (2010)

6. Acknowledgements

This work was funded by the Federal Ministry of Education and Research (BMBF InnoProfile-Transfer 20118311) and the German Research Foundation (DFG Grant WI 4140/2-1). The authors wish to thank Comsol Multiphysics GmbH for providing a test version of the Floating Network License of COMSOL Multiphysics® 5.1 as well as for technical support.